Investigation of the Hydrothermal Crystallisation of the Perovskite Solid Solution $NaCe_{1-x}La_xTi_2O_6$ and its Defect Chemistry

Mohammad H. Harunsani[1], David I. Woodward[2], Martin D. Peel[3], Sharon E. Ashbrook[3] and Richard I. Walton[1*]

[1]Department of Chemistry, University of Warwick, Coventry, CV4 7AL, U.K.
*email: r.i.walton@warwick.ac.uk

[2]Department of Physics, University of Warwick, Coventry, CV4 7Al, U.K.

[3]School of Chemistry, and EaStCHEM University of St Andrews, North Haugh, St Andrews, KY16 9ST, U.K.

Abstract. Perovskites of nominal composition $NaCe_{1-x}La_xTi_2O_6$ ($0 \leq x \leq 1$) crystallise directly under hydrothermal conditions at 240 ^{o}C. Raman spectroscopy shows distortion from the ideal cubic structure and Rietveld analysis of powder X-ray and neutron diffraction reveals that the materials represent a continuous series in rhombohedral space group $R\bar{3}c$. Ce L_{III}-edge X-ray absorption near edge structure spectroscopy shows that while the majority of cerium is present as Ce^{3+} there is evidence for Ce^{4+}. The paramagnetic Ce^{3+} affects the chemical shift and line width of ^{23}Na MAS NMR spectra, which also show with no evidence for A-site ordering. ^{2}H MAS NMR of samples prepared in D_2O shows the inclusion of deuterium, which IR spectroscopy shows is most likely to be as D_2O. The deuterium content is highest for the cerium-rich materials, consistent with oxidation of some cerium to Ce^{4+} to provide charge balance of A-site water.

Keywords: Perovskite; hydrothermal; XANES; NMR; neutron diffraction

Graphical Abstract

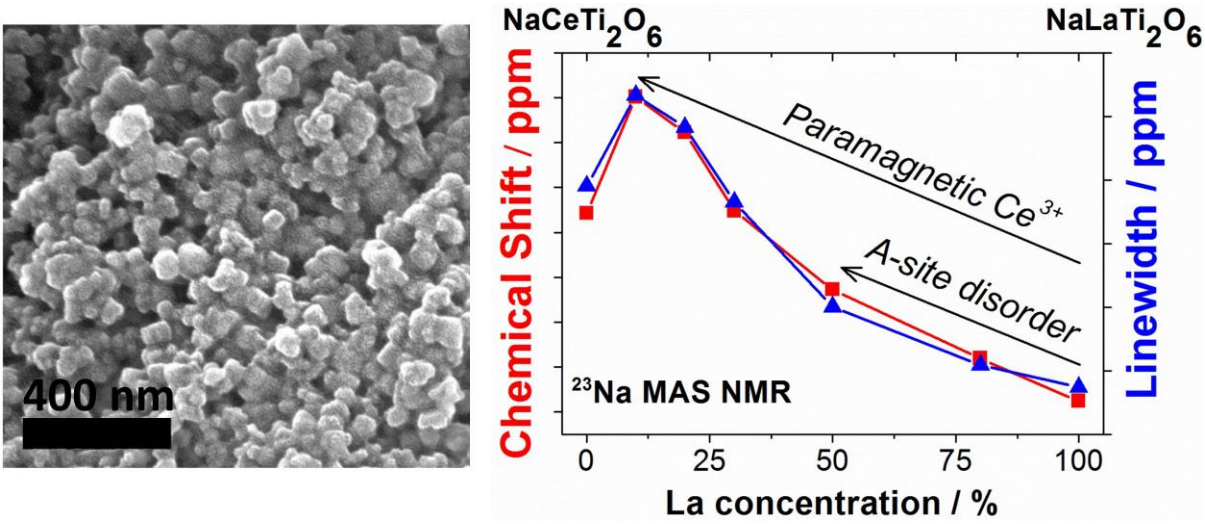

A multi-element A-site perovskite crystallises directly from aqueous, basic solutions at 240 ºC; while the paramagnetic effect of Ce^{3+} on the ^{23}Na NMR shows a homogeneous solid-solution, the incorporation of A-site water is also found from ^{2}H NMR and IR, with oxidation of some cerium to charge balance proved by XANES spectroscopy.

1. Introduction

Mixed-metal oxides are important materials with wide-ranging properties of relevance for a number of well-established applications, such as in areas of electronics, magnetism, ferroelectrics and catalysis [1-4]. Among the mixed metal oxides, ABO_3 perovskites stand out due to their versatility in terms of both their chemical composition and structural flexibility [5, 6]. The ideal cubic perovskite structure consists of a network of corner-shared BO_6 octahedra in which all 12-coordinate interstitial sites are filled by A-site metals [7].The structure can accommodate most metal ions, and partial substitution on the A and B sites is also possible, with distortion possible by concerted rotation of octahedra about their common oxide bridges so to lower the coordination of the A-site to accommodate smaller ions. Local distortion of the octahedra themselves is also possible, such as off-centre displacement of the B-site metal cations. This results in practical applications that have high commercial value. For example, $BaTiO_3$ and lead zirconium titanate, $PbZr_xTi_{1-x}O_3$, have ferroelectric properties and are widely used to make capacitors [8, 9]. Owing to the toxicity of lead, there have been an increasing number of studies trying to develop alternative materials for these important applications, such as solid solutions based on the perovskites $Na_{0.5}Bi_{0.5}TiO_3$ and $NaNbO_3$ [10-13].

Perovskite oxides are commonly prepared by solid-state synthesis, where high temperatures above 1000 ^oC are used for extended periods of time to bring about reaction between solid oxide or carbonate precursors. Such approaches give highly crystalline products, however, they provide very little control over the particle size and usually only give the most thermodynamically stable products. Hydrothermal synthesis provides a convenient, low-temperature route to mixed-metal oxide materials [14-18]. For example, the perovskites $BaTiO_3$ and $SrTiO_3$ can be crystallised directly at 80-100 ^oC from metal salts in basic solution [19, 20].The preparation of more complex oxides, more challenging by solid-state synthesis where inhomogeneity can result [21], can also be performed hydrothermally in a single step (*i.e.*, without any high temperature annealing needed to bring about crystallisation); examples include $Ba_{1-x}Sr_xTiO_3$ [22, 23] and $Ln_{1-x}B_xMnO_3$ (Ln = La,Pr and B = Ba,Sr,Ca) [24-28]. By using temperatures below 250 ^oC and solutions of reagents in a sealed reaction vessel, the hydrothermal technique ensures that the reagents are well mixed to give homogeneous products and the solvent-mediated crystal growth provides control over the particle size and morphology of the products. This may be important in areas such as catalysis, where

nanoscale crystallites are often desired, and in electronic or magnetic applications, where the preparation of fine-grained ceramics is possible by sintering the as-made powders. The low reaction temperature may also prevent the loss of volatile metals such as Bi and Na, which occurs readily at elevated temperatures, giving compositionally homogeneous materials. The crystal morphology of the materials can also be controlled by replacing water with other solvents. For example, hollow cubes and spheres of $CaTiO_3$ can be made solvothermally in polyethylene glycol [29, 30], and ethylenediamine and ethanolamine have been used to adjust the morphology of $Ba_{1-x}Sr_xTiO_3$ from spherical to cube-shaped particles [31].

This paper is concerned with the preparation of the Ce and La analogues of $Na_{0.5}Bi_{0.5}TiO_3$ by hydrothermal synthesis. $NaLaTi_2O_6$ exhibits a dielectric property, known as quantum paraelectricity, at low temperatures, where samples prepared by conventional solid-state reactions have been studied [32, 33]. $NaCeTi_2O_6$ is a synthetic analogue of the mineral loparite and has been prepared using hydrothermal synthesis by Wright *et al.*, who reacted $CeCl_3{\cdot}7H_2O$ and TiF_3 in 4 M NaOH solution at temperatures above 100 ^oC, and also prepared Nd and V doped analogues[34], while cubic particles of $NaLaTi_2O_6$ were prepared hydrothermally by Shi *et al.* from TiN and $La(NO_3)_3{\cdot}6H_2O$ [35].The aim of the present study was to investigate the scope for the preparation of complex perovskite solid solutions from these end members, to prove the degree of element mixing using a variety of structural probes, and to investigate the level of defects in the hydrothermally prepared samples.

2. Experimental Section

Material synthesis. Hydrothermal syntheses of the samples were performed using ~20 mL Teflon-lined stainless steel autoclaves. The reagents used were: $CeCl_3{\cdot}7H_2O$ (Sigma Aldrich, 99.9%), $LaCl_3{\cdot}7H_2O$ (Alfa, 99%) and TiF_3 (Alfa, 98%). The exact amount of water in the salts was determined by thermogravimetric analysis. The three reagents were stirred in 5 mL of deionised water for 5 min in a Teflon liner before 5 mL of NaOH solution (either 4 M or 12 M) was added and then stirred for 1 hour. The reaction vessel was then sealed in the steel autoclave and placed in an oven pre-heated at 240 ^oC for 24 hours and then allowed to cool to room temperature. The solid products were recovered by suction filtration, washed thoroughly with warm water and dried overnight in a drying oven. The products were then ground into powder for further characterisation. Deuterated samples of $NaCeTi_2O_6$ and

$NaLaTi_2O_6$ were prepared using the same procedure as above but using D_2O and NaOD. The aim here was to prepare samples for solid-state NMR to investigate the level of defects in the samples, thus samples once crystallised were washed with copious amounts of deionised H_2O to ensure that any surface D_2O or $[OD]^-$ was removed and that any remaining deuterium was present only within the crystal structure. Solvothermal reactions were also carried out, where ethylene glycol was used to replace water as the solvent. $CeCl_3.7H_2O$ / $LaCl_3.7H_2O$ and TiF_3 were mixed with stirring in 5 mL ethylene glycol for 15 min, then 1.6 g NaOH was added and the mixture stirred for 1 hr. The reaction vessel was then sealed and heated at 240 ^oC for 24 hr. Reactions with a 1:1 mixture of H_2O and ethylene glycol were prepared by mixing the reagents in 2 mL deionised water, then 3 mL NaOH (4 M) was added and the mixture stirred for 15 min. Then 5 mL ethylene glycol was added and stirred for 1 hour before being sealed and heated at 240 ^oC for 24 hr.

Characterisation. Powder X-ray diffraction (XRD) data were collected using a Panalytical X-Pert Pro MPD diffractometer (Cu $K_{\alpha 1}$ radiation). Neutron powder data were collected at room temperature on diffractometer D2B at the Institut Laue-Langevin, Grenoble, France, where the samples were loaded into a cylindrical vanadium canister and a wavelength of 1.594 Å was used. The data collection times for neutron diffraction were typically around 6 hours and Rietveld analysis of diffraction data was performed using the *TOPAS* software [36]. Raman spectroscopic data were recorded at room temperature using Renishaw inVia Raman Microscope equipped with an Ar^+ laser with wavelength 514.5 nm and Renishaw CCD detectors. SEM images of the samples were recorded using Zeiss SUPRA 55VP FEG scanning electron microscope. A working distance of 3 mm and a gun voltage of 20 kV were used. Energy Dispersive X-ray Analysis was also performed using the SEM in order to determine the elemental composition of the materials. IR spectra were recorded from the solid samples using a Perkin-Elmer Spectrum100 diamond ATR-FTIR spectrometer. ICP analysis for metals was performed by Medac Ltd (UK).

Solid-State NMR. Solid-state NMR spectra were acquired using a Bruker 600 Avance III spectrometer, equipped with a wide-bore 14.1 T magnet, giving Larmor frequencies of 158.7 MHz for ^{23}Na (I = 3/2) and 92.1 MHz for ^2H (I = 1). Powdered samples were packed into conventional 4-mm ZrO_2 rotors, and a magic-angle spinning (MAS) rate of 12.5 kHz was employed. ^{23}Na chemical shifts were referenced to 1 M $NaCl_{(aq)}$ using a secondary reference $NaCl_{(s)}$ (δ_{iso} = 7.8 ppm), and ^2H chemical shifts were referenced to deuterated

tetramethylsilane, using the OD resonance of fully deuterated malonic acid (δ_{iso} = 13.0 ppm) as a secondary reference. Conventional ^{23}Na and ^{2}H MAS NMR spectra were obtained using single-pulse experiments at 14.1 T, with typical pulse lengths of 1.5 and 4 μs, respectively. Recycle intervals of 5 and 3 s were used for ^{23}Na and ^{2}H, respectively, with a radiofrequency nutation rate of ~100 kHz and ~50 kHz, respectively. Further experimental details can be found in the relevant figure captions.

Ce L_{III}-edge XANES. Ce L_{III}-edge X-ray absorption fine structure (XANES) experiments were performed using beamline B18 of the Diamond Light Source, UK [37]. This beamline provides X-ray energies in the range 2.05 - 35 keV using a fixed-exit, double-crystal Si(111) monochromator, which provides an energy resolution ($\Delta E/E$) of 2×10^{-4}. The optics of the beamline includes a collimating mirror and a toroidal focussing mirror before and after the monochromator, respectively. The measurements presented here were carried out using the Cr coating of these two optical elements and a pair of harmonic rejection mirrors with a Ni stripe were also used. Under this configuration, the typical flux on the sample is of the order of 5×10^{11} photons s^{-1} and the size of the beam at that position is approximately 200 μm (vertical) by 150 μm (horizontal). The samples were ground finely with polyethylene powder (~ 80% by mass as diluent) under acetone to achieve uniform dispersion and pressed into 13 mm diameter pellets of ~1 mm thickness under a pressure of 5 tonnes. The reference materials CeO_2 (used as provided by Sigma Aldrich) and $CeAlO_3$ (prepared by solid-state reaction between Al_2O_3 and CeO_2 at 1450 °C under a flow of 5 % H_2 in N_2 for 10 hours) provided examples of cerium with well-defined oxidation states and coordination environments. XANES data were collected in transmission mode with ion chambers before and behind the sample filled with appropriate mixtures of inert gases to optimise sensitivity. The spectra were measured with a step size equivalent to less than 0.5 eV. Data were normalised using the program Athena [38] with a linear pre-edge and polynomial post-edge background subtracted from the raw $\ln(I_t/I_0)$ data.

3. Results and Discussion

X-ray diffraction (XRD) studies were carried out to confirm that the hydrothermal synthesis of the complete series of $NaCe_{1-x}La_xTi_2O_6$, for the range $0 \leq x \leq 1$ was successful. $NaCeTi_2O_6$ has been reported to have an orthorhombic *Pnma* structure [34, 39] while several

different structures have been reported for $NaLaTi_2O_6$ at room temperature including cubic [32], rhombohedral [40, 41], tetragonal [42] and orthorhombic [33, 43, 44] unit cells. Ranjan *et al.* [40] attributed the contradicting reports for $NaLaTi_2O_6$ in the literature to the fact that the distortion of the perovskite structure is weak and that other authors had used only X-ray diffraction data for structure analysis. They collected powder neutron diffraction data and by using Rietveld refinement showed that $NaLaTi_2O_6$ prepared by solid-state synthesis has a structure best described with the rhombohedral, $R\bar{3}c$, space group [40].

The powder XRD data collected for the $NaCe_{1-x}La_xTi_2O_6$ series agree with the structure reported for $NaLaTi_2O_6$ with space group $R\bar{3}c$. However, the weak peaks caused by slight distortions in the perovskite structure could not be resolved by X-ray diffraction. Weak peaks expected for rhombohedral $R\bar{3}c$ were observed, however, in the neutron diffraction data, which are more sensitive to oxygen atomic positions than X-rays in these metal oxides. Although the end member $NaCeTi_2O_6$ has been reported in the literature with the space group *Pnma* [34, 39] there were fewer peaks observed in the neutron diffraction pattern than were expected for this model. A tetragonal model (*I*4/*mcm*) was also tested but it gave a slightly poorer fit than the $R\bar{3}c$ model. The neutron diffraction data and the final Rietveld refinement fits for the materials $NaCeTi_2O_6$, $NaCe_{0.5}La_{0.5}Ti_2O_6$ and $NaLaTi_2O_6$ are shown in Fig. 1 using the $R\bar{3}c$ model, with the refined structural parameters given in Table 1. The formation of a solid solution can be confirmed by changes in the cell parameters, shown in Fig. 2. Both the *a* and *c* lattice parameters increase as the La concentration is increased; this is due to La^{3+} ions (1.36 Å) having a larger ionic radius than Ce^{3+} (1.34 Å) [45].

In the literature, there are no reports found on the Raman spectrum of $NaCeTi_2O_6$ but there have been several reports for $NaLaTi_2O_6$ [35, 46, 47]. The Raman spectroscopic data shown in Fig. 3 confirm that the structures of the samples all have distortions from the ideal cubic aristotype perovskite as no first-order Raman bands are expected for cubic symmetry. The spectra show broad bands consistent with other reports for $NaLaTi_2O_6$ and for related perovskites such as $Na_{0.5}Bi_{0.5}TiO_3$ [42, 46, 48-50]. This broadening may be due to the disorder on the A-site and the overlapping of multiple Raman modes. The main bands for all the samples are observed at approximately 150, 260, 450, 550 and 830 cm^{-1}. The band at 150 cm^{-1}, assigned to modes of A_1 symmetry, has been attributed to Na-O vibrations [51]. The band at around 260 cm^{-1}, also assigned to modes of A_1 symmetry, increases in intensity relative to that at 150 cm^{-1} with increasing La content. This band is also observed in the

Raman spectra of $BaTiO_3$ and $PbTiO_3$ at almost the same position, indicating that it is dominated by Ti-O vibrations [51]. The band at around 450 cm^{-1}, which is most prominent in $NaLaTi_2O_6$, increases in intensity when $NaLaTi_2O_6$ is annealed. This band has been correlated to the particle size of $NaLaTi_2O_6$; Zhang *et al.* observed an increase in the intensity of this peak with increasing $NaLaTi_2O_6$ particle size from 14 to 50 nm [47].

High-frequency Raman bands in oxides are usually dominated by vibrations involving oxygen displacements so the band at around 550 cm^{-1} has been reported to be due to TiO_6 octahedral vibrations and assigned to a mixture of A_1 and E modes [42, 51, 52]. For $Na_{0.5}Bi_{0.5}TiO_3$, with space group *R*3*c*, there are 13 Raman active modes and they are all observed below 700 cm^{-1}, while the high-temperature $LaGaO_3$, which has the same space group ($R\bar{3}c$) as $NaLaTi_2O_6$, is expected to have 5 Raman active modes (52, 160, 252 and 444 cm^{-1}) that are also observed below 700 cm^{-1} [53, 54]. Most Raman studies for $NaLaTi_2O_6$ and $Na_{0.5}Bi_{0.5}TiO_3$ only provide Raman data below 700 cm^{-1} so the last broad band at around 830 cm^{-1} is not usually reported. Selvamani *et al.* have reported an increase in the intensity of the band at 830 cm^{-1} as more $BiCrO_3$ is doped into $Na_{0.5}Bi_{0.5}TiO_3$ and have attributed this band to the presence of oxygen vacancies [55]. In the Raman spectra of $(Li_xNa_{1-x})NbO_3$, a band at 875 cm^{-1} was observed, where it was assigned to an impurity band by Yuzyuk *et al.* [56] but to an overtone by Juang *et al.* [57]. In the case of tetragonal $BaTiO_3$, Raman bands above 700 cm^{-1} have been reported, where the band at 720 cm^{-1} is assigned to a mixture of E and A_1 mode while the band at 810 cm^{-1} may arise from the deformation of lattice OH groups as it was not present after annealing at 700 ^oC [58, 59]. However, $NaLaTi_2O_6$ still exhibits the broad band at around 830 cm^{-1} even after annealing.

Fig. 4 shows SEM images of $NaCe_{1-x}La_xTi_2O_6$ powders prepared by hydrothermal synthesis using 4 M NaOH. The particles have irregular shapes with particle size around 100 nm. There is little change in morphology between $NaCeTi_2O_6$ and $NaLaTi_2O_6$. A degree of control of the particle size, however, was achieved by altering the solvent, or by increasing the NaOH concentration, as shown in Fig. 5. By changing the solvent from water to ethylene glycol, the particle size of the product is clearly reduced, whilst the particle size was increased when the NaOH concentration was increased from 4 M to 12 M. The morphology of $NaCeTi_2O_6$ and $NaLaTi_2O_6$ particles became more spherical when a 1:1 mixture of H_2O and ethylene glycol was used as shown in Figs 5e and 5f. The atomic composition of the

samples was determined by EDXA on the SEM and as shown in Table 2, and reasonable agreement was found between the intended and expected atomic percentages of metals.

The Ce L_{III}-edge XANES spectra of $NaCeTi_2O_6$ prepared using different reaction times or concentrations of NaOH are shown in Fig. 6, along with those for the materials $CeAlO_3$ and CeO_2, where the Ce has oxidation state of +3 and +4, respectively. For the cerium (III) oxide a single white line is seen, corresponding to the electronic transition $2p_{3/2} \rightarrow (4f^{1})5d$, whereas the spectrum of the cerium (IV) oxide shows a typical double feature comprising of $2p_{3/2} \rightarrow (4f\underline{L})5d$ and $2p_{3/2} \rightarrow (4f^{0})5d$ transitions, with an absorption edge shift of ~ 5 eV to higher energy [60-62]. The material $CeAlO_3$ is a tetragonal (*I*4/*mcm*) perovskite [63], which contains cerium (III) in a similar environment to that expected in the rhombohedral $NaCeTi_2O_6$ we have studied. The XANES spectra of the $NaCeTi_2O_6$ samples, and the $NaCe_{0.5}La_{0.5}Ti_2O_6$ material, all show distinct differences from the $CeAlO_3$ reference, with some evidence for the presence of Ce^{4+} in addition to the predominant Ce^{3+}: this is clear from the observation of a weak higher energy $2p_{3/2} \rightarrow (4f^{0})5d$ feature, an asymmetry of the white line in the region of the $2p_{3/2} \rightarrow (4f\underline{L})5d$ transition, as indicated on Fig. 6, and a shift of the absorption edge to higher energy. It is noteworthy that the sample of $NaCeTi_2O_6$ prepared at the shortest reaction time with the lower concentration of NaOH appears to show less evidence for presence of Ce^{4+} (note this is the sample whose structure refinement is described above). The previously published XANES spectrum of hydrothermal $NaCeTi_2O_6$ was compared only with cerium (III) chloride [34]; our new comparison with $CeAlO_3$ provides clear evidence for the partial oxidation of cerium in apparently stoichiometric $NaCeTi_2O_6$. Since the intensity of the white line depends on the coordination number and local geometry about cerium, the position of the absorption edge (simply defined as the energy of 50 % of the edge step) provides the most convenient means of quantifying the oxidation state of cerium. Assuming a linear correlation between edge position and oxidation state [34], then we can estimate that the oxidation state of cerium in the $NaCeTi_2O_6$ materials is +3.2 in the material prepared in 4 M NaOH for short reaction time (*i.e.*, 20 % of the cerium is present as Ce^{4+}) and reaches +3.4 in the material prepared in 12 M NaOH. Since the high-resolution powder diffraction experiments show no evidence for crystalline CeO_2 impurities in the samples, three possible explanations for the presence of Ce^{4+} may be put forward: (1) amorphous CeO_2 is present, (2) the surface of the fine powders contains oxidised cerium or (3) cerium is oxidised within the perovskite structure to accommodate structural defects (see below).

The samples were studied by ^{23}Na NMR to examine the level of A-site ordering. The chemical shift of Na in a site with high coordination number, such as in a perovskite, should be close to 0 ppm [64-66], which is the case for all the samples studied. The chemical shift and line width varies across the series, however, as shown in Fig. 7. When the chemical shift and linewidth are plotted against the La concentration, the trend in both cases is identical. There are two effects that may be responsible for the trends seen. One arises from the presence of paramagnetic Ce^{3+} (resulting in paramagnetic contributions to both linewidth and shift of the Na resonance), and the other is from the disorder due to the three different metals occupying the A-site (again with potential contributions to linewidth, through a distribution of local environments, and to the shift as the neighbouring cations vary). It is, therefore, expected that $NaLaTi_2O_6$ should have the narrowest peak width since there is no paramagnetic Ce in the material, and there is less local disorder, with only two A-site metals present. As the La concentration is lowered with cerium added to the material, the potential for disorder increases with three A-site metal cations present, and a broadening of the resonance is expected. If the A-site disorder is the only effect on the linewidth, then the $NaCe_{0.5}La_{0.5}Ti_2O_6$ sample should have the broadest peak (*i.e.*, maximum disorder if no clustering or ordering is present). However, the peaks continue to broaden across the series until the $NaCe_{0.9}La_{0.1}Ti_2O_6$ composition is reached. This can be understood in terms of the additional contribution to the linewidth of paramagnetic broadening from the Ce^{3+}. The linewidth then drops slightly at $NaCeTi_2O_6$ as there are only two A-site metals and hence, less A-site disorder.

For comparison, ^{23}Na NMR spectra of physical mixtures of $NaCeTi_2O_6$-$NaLaTi_2O_6$ were also obtained. The physical mixtures with 20% and 50% $NaLaTi_2O_6$ showed considerably less peak broadening compared to the samples made hydrothermally, as shown in Fig. 8. This indicates that when the Ce^{3+} is not incorporated into the same structure as La, no paramagnetic effects are observed on the Na signal resulting from this phase. This is consistent with the fact that the samples made hydrothermally are a genuine solid solution, with an intimate mixture of A-site metal cations, rather than simply physical mixtures of the oxides.

We now consider the possibility of water or hydroxide being incorporated in the perovskite structure. In Fig. 9 it can be seen that the ^{2}H NMR spectra of both of the deuterated perovskites made in D_2O / NaOD give a small but significant NMR signal. In

order to ensure that the low intensity signal observed did not result from natural-abundance levels of ^2H in the background the probe/rotor, experiments were also conducted for empty rotors. No signal was observed, confirming that the ^2H signal seen in Fig. 9 does indeed result from ^2H trapped within the perovskite structure. Once the deuterated $NaLaTi_2O_6$ was then heated above 900 ^oC, the signal was not observed by ^2H NMR suggesting that the deuterium-containing species, although within the crystals, can be removed on heating. The presence of water and hydroxide in hydrothermally prepared oxides has been reported by other authors. Goh *et al.* observed two separate signals in the ^1H NMR spectrum of $KNbO_3$ prepared hydrothermally [67]. They attributed the two signals to the presence of both water and hydroxyl ions in the perovskite lattice. Chien *et al.* performed ^2H NMR on deuterated $BaTiO_3$ to detect the presence of $[OD]^-$ groups within the $BaTiO_3$ lattice (on oxide sites), showing a single narrow peak with a broad, overlapping component [68]. They attributed the narrow peak to D_2O trapped between the $BaTiO_3$ crystallites, or close to the surface of the crystals, while the broad component is due to D_2O or $[OD]^-$ trapped within the $BaTiO_3$ lattice; thus our results are rather similar. The ^2H resonance for $NaCeTi_2O_6$ is slightly shifted compared to $NaLaTi_2O_6$. This is undoubtedly because of the effect of paramagnetic Ce, similar to the small shift found in the ^{23}Na NMR spectra. This also suggests that the deuterated species are within the perovskite structure since they are influenced by the paramagnetic effect of Ce^{3+}.

The amount of deuterium within the samples can, in principle, be quantified using NMR spectroscopy, by comparing the ^2H signal obtained from the sample (when a known number of transients were averaged) to that obtained from a natural-abundance sample of a known amount of water. Thus, the concentration (mmol/g) and then a percentage by weight of ^2H in each sample can be determined. For $NaLaTi_2O_6$, we calculate 1.7 mmol/g ^2H for the centreband signal and a further 1.4 mmol/g from the sidebands, therefore 0.6 % ^2H by weight. For $NaCeTi_2O_6$, the sidebands are broad and too low in intensity to integrate but by integrating the sharp centreband we determine 13.88 mmol/g ^2H to be present in the centreband, which by weight gives 2.8% ^2H. Although many assumptions have been made in these calculations and the errors are large, we can clearly deduce that a significantly larger amount of deuterium is incorporated in the crystal structure of the $NaCeTi_2O_6$ compared to $NaLaTi_2O_6$. To rationalise this observation, the presence of Ce^{4+}, seen by XANES, can be used: the extra charge of the Ce^{4+} may be balanced by removal of sodium from the A-site, which is then replaced by D_2O molecules. ICP analysis for metals produces a consistent picture: the nominal $NaCeTi_2O_6$ material is best formulated as $(Na_{0.7}Ce_{0.9}(H_2O)_{0.4})Ti_2O_6$

(observed 4.77 % Na, 35.71 % Ce and 27.36 % Ti, calculated 4.71 % Na, 36.96 % Ce and 28.07 % Ti). This formulation results in an average Ce oxidation state +3.6, slightly higher but not inconsistent with the XANES analysis described above, while for the nominal $NaLaTi_2O_6$ material the formula $(Na_{0.7}La_{1.1}(H_2O)_{0.2})Ti_2O_6$ best fits the observed analysis (observed 4.46 % Na, 40.26 % La and 27.72 % Ti and calculated 4.41 % Na, 41.95 % La and 26.29 % Ti, with the La oxidation maintained at +3, as expected). Thus the cerium-containing phase is able to accommodate more A-site water than the lanthanum containing material. As a final verification of this idea, the occupancy of the A site was investigated in Rietveld refinement against the powder X-ray diffraction data, Table 3. This shows that inclusion of oxygen as a third A-site component (representing a water molecule) and refinement of the occupancy of each species gives a composition consistent with the presence of water at the expense of sodium. This also gave a smaller improvement in the overall fit and, importantly resulted in physically meaningful temperature factors for all sites, which was not the case for the simple model without inclusion of water. We note also that the refinement predicts most water present in the $NaCeTi_2O_6$ end member, entirely consistent with the spectroscopic results presenetd above. The presence of water molecules on the A-site of a perovskite is not unprecedented; for example, it has been reported for a barium potassium bismuthate perovskite, also prepared by hydrothermal synthesis [69].

The IR spectra of $NaLaTi_2O_6$ and $NaCeTi_2O_6$ in Fig. 10 show absorption bands due to O-H stretching at around 3400 cm^{-1}. This band was not observed in sintered $NaLaTi_2O_6$ confirming that all the O-H containing species are removed upon heating (note that sintering $NaCeTi_2O_6$ causes phase separation so IR of that sample was not recorded). Similar results are reported in the literature for perovskites prepared hydrothermally [58, 68, 70, 71]. Noma *et al.* observed a sharp band at around 3500 cm^{-1} in hydrothermal $BaTiO_3$, which they attributed to lattice hydroxyl groups occupying the oxide sites, and a broad band from 3000-3600 cm^{-1} which was ascribed to surface-adsorbed hydroxyl groups, present either as hydroxide or as water. In our perovskite samples, no sharp bands are observed in this region of the IR, Figure 10, which suggests minimal incorporation of hydroxide within the lattice. Therefore, the broad band we observe must be due to some more weakly bound proton-containing species. This we propose is the A-site water deduced from the NMR studies.

4. Conclusions

The perovskite solid solution with nominal composition $NaCe_{1-x}La_xTi_2O_6$ over the whole composition range has been successfully prepared under hydrothermal conditions. All the samples are assigned the space group $R\bar{3}c$, which matches $NaLaTi_2O_6$ previously prepared by solid-state synthesis, and the lattice parameters show a linear increase with increasing La concentration. The effect of changing the solvent and NaOH concentration showed that particle size was reduced by using ethylene glycol as the solvent, while an increase in the particle size was achieved using higher NaOH concentrations. ^{23}Na MAS NMR confirms that the materials produced are a genuine solid solution where the three A-site metals are randomly arranged, where the effect of paramagnetic Ce^{3+} proves the intimate mixing of substituent metals. XANES spectra recorded at the Ce L_{III}-edge show clearly that the materials all contain some degree of Ce^{4+}, and the presence of varying amounts of this ion, depending on synthesis conditions, may provide a means of balancing the charge of defects seen by ^{2}H MAS NMR and IR. All analysis results produce a consistent picture of the inclusion of A-site water in the hydrothermally-synthesised materials, which can be accommodated to a greater extent by the oxidation of some Ce^{3+} to Ce^{4+}. This compositional variation may explain the different crystal symmetry seen for various specimens of assumed composition $NaLaTi_2O_6$ and $NaCeTi_2O_6$ reported in the literature, especially from specimens prepared by different methods.

5. Acknowledgements

Some of the equipment used in materials characterisation at the University of Warwick was obtained through the Science City Advanced Materials project "Creating and Characterising Next Generation Advanced Materials" with support from Advantage West Midlands (AWM) and part funded by the European Regional Development Fund (ERDF). We are grateful for the STFC for provision of beamtime at Diamond Light Source, and we thank Dr Silvia Ramos for her assistance with measuring the XANES data on B18. MHH thanks the Ministry of Education, Brunei for award of a scholarship. EPSRC are thanked for a DTG studentship to MDP. We are grateful to Dr Emmanuelle Suard for her help with measuring neutron diffraction data at ILL.

References

[1] N. Izyumskaya, Y. Alivov, H. Morkoc, Crit. Rev. Solid State Mater. Sci., 34 (2009) 89-179.
[2] G. Arlt, D. Hennings, G. Dewith, J. Appl. Phys., 58 (1985) 1619-1625.
[3] J. Wang, J.B. Neaton, H. Zheng, V. Nagarajan, S.B. Ogale, B. Liu, D. Viehland, V. Vaithyanathan, D.G. Schlom, U.V. Waghmare, N.A. Spaldin, K.M. Rabe, M. Wuttig, R. Ramesh, Science, 299 (2003) 1719-1722.
[4] M.M. Bettahar, G. Costentin, L. Savary, J.C. Lavalley, Appl. Catal. A - General, 145 (1996) 1-48.
[5] M.A. Pena, J.L.G. Fierro, Chem. Rev., 101 (2001) 1981-2017.
[6] R.H. Mitchell, *Perovskites: Modern and Ancient*, Almaz Press Inc., Thunder Bay, ON, Canada, , 2002.
[7] A.F. Wells, *Structural Inorganic Chemistry*, 5th Edition, Oxford University Press, Oxford, 1984.
[8] G.H. Haertling, J. Am. Ceram. Soc., 82 (1999) 797-818.
[9] T.R. Shrout, S.J. Zhang, J. Electroceram., 19 (2007) 113-126.
[10] K. Datta, P.A. Thomas, K. Roleder, Phys. Rev. B, 82 (2010).
[11] V.A. Isupov, Ferroelectrics, 315 (2005) 123-147.
[12] J.E. Daniels, W. Jo, J. Rodel, V. Honkimaki, J.L. Jones, Acta Mater., 58 (2010) 2103-2111.
[13] J.F. Li, K. Wang, B.P. Zhang, L.M. Zhang, J. Am. Ceram. Soc., 89 (2006) 706-709.
[14] R.I. Walton, Chem. Soc. Rev., 31 (2002) 230-238.
[15] S. Somiya, R. Roy, Bull. Mater. Sci., 23 (2000) 453-460.
[16] G. Demazeau, J. Mater. Chem., 9 (1999) 15-18.
[17] D.R. Modeshia, R.I. Walton, Chem. Soc. Rev., 39 (2010) 4303-4325.
[18] R.E. Riman, W.L. Suchanek, M.M. Lencka, Annal. Chim.-Sci.Mater., 27 (2002) 15-36.
[19] S.S. Flaschen, J. Am. Chem. Soc., 77 (1955) 6194.
[20] N. Ishizawa, H. Banno, S. Hayashi, S.E. Yoo, M. Yoshimura, Jpn. J. Appl. Phys., 29 (1990) 2467-2472.
[21] Y. Mao, T.J. Park, S.S. Wong, Chem. Commun., (2005) 5721-5735.
[22] R.Z. Hou, A.Y. Wu, P.A. Vilarinho, Chem. Mater., 21 (2009) 1214-1220.
[23] B.L. Gersten, M.M. Lencka, R.E. Riman, J. Am. Ceram. Soc., 87 (2004) 2025-2032.
[24] J. Spooren, R.I. Walton, F. Millange, J. Mater. Chem., 15 (2005) 1542-1551.
[25] Y. Chen, H.M. Yuan, G. Tian, G.H. Zhang, S.H. Feng, J. Solid State Chem., 180 (2007) 167-172.
[26] J.G. Deng, L. Zhang, H.X. Dai, C.T. Au, Catal. Lett., 130 (2009) 622-629.
[27] J.J. Urban, L. Ouyang, M.H. Jo, D.S. Wang, H. Park, Nano Lett., 4 (2004) 1547-1550.
[28] T. Zhang, C.G. Jin, T. Qian, X.L. Lu, J.M. Bai, X.G. Li, J. Mater. Chem., 14 (2004) 2787-2789.
[29] X.F. Yang, I.D. Williams, J. Chen, J. Wang, H.F. Xu, H.M. Konishi, Y.X. Pan, C.L. Liang, M.M. Wu, J. Mater. Chem., 18 (2008) 3543-3546.
[30] X.F. Yang, J.X. Fu, C.J. Jin, J.A. Chen, C.L. Liang, M.M. Wu, W.Z. Zhou, J. Am. Chem. Soc., 132 (2010) 14279-14287.
[31] X. Wei, G. Xu, Z.H. Ren, Y.G. Wang, G. Shen, G.R. Han, J. Cryst. Growth, 310 (2008) 4132-4137.
[32] Y. Inaguma, J.H. Sohn, I.S. Kim, M. Itoh, T. Nakamura, J. Phys. Soc. Jpn., 61 (1992) 3831-3832.
[33] P.H. Sun, T. Nakamura, Y.J. Shan, Y. Inaguma, M. Itoh, Ferroelectrics, 200 (1997) 93-107.

[34] C.S. Wright, R.I. Walton, D. Thompsett, J. Fisher, Inorg. Chem., 43 (2004) 2189-2196.
[35] J.W. Shi, J.H. Ye, Z.H. Zhou, M.T. Li, L.J. Guo, Chem. Eur. J, 17 (2011) 7858-7867.
[36] A.A. Coelho, J.S.O. Evans, I.R. Evans, A. Kern, S. Parsons, Powder Diffr., 26 (2011) S22-S25.
[37] A.J. Dent, G. Cibin, S. Ramos, A.D. Smith, S.M. Scott, L. Varandas, M.R. Pearson, N.A. Krumpa, C.P. Jones, P.E. Robbins, in *14th International Conference on X-Ray Absorption Fine Structure (XAFS14)*, Camerino, Italy, 2009.
[38] B. Ravel, M. Newville, J. Synchrotron Rad., 12 (2005) 537.
[39] A.R. Chakhmouradian, R.H. Mitchell, A.V. Pankov, N.V. Chukanov, Mineral. Mag., 63 (1999) 519-534.
[40] R. Ranjan, A. Senyshyn, H. Boysen, C. Baehtz, F. Frey, J. Solid State Chem., 180 (2007) 995-1001.
[41] R. Garg, A. Senyshyn, H. Boysen, R. Ranjan, J. Phys. Cond. Matt., 20 (2008) 6.
[42] Y. Li, S. Qin, F. Seifert, J. Solid State Chem., 180 (2007) 824-833.
[43] R.H. Mitchell, A.R. Chakhmouradian, J. Solid State Chem., 138 (1998) 307-312.
[44] M.C. Knapp, P.M. Woodward, J. Solid State Chem., 179 (2006) 1076-1085.
[45] R.D. Shannon, Acta Crystallogr. A, 32 (1976) 751-767.
[46] M.L. Sanjuan, M.A. Laguna, A.G. Belous, O.I. V'Yunov, Chem. Mater., 17 (2005) 5862-5866.
[47] W.F. Zhang, X.T. Zhang, H. Guo, J.L. Fang, M.S. Zhang, Chem. J. Chin. Univ., 20 (1999) 515-518.
[48] S. Trujillo, J. Kreisel, Q. Jiang, J.H. Smith, P.A. Thomas, P. Bouvier, F. Weiss, J. Phys. Cond. Matt., 17 (2005) 6587-6597.
[49] B.K. Barick, K.K. Mishra, A.K. Arora, R.N.P. Choudhary, D.K. Pradhan, J. Phys. D, 44 (2011).
[50] W.F. Zhang, Z. Yin, M.S. Zhang, J.L. Fang, J. Mater. Sci. Lett., 18 (1999) 813-815.
[51] J. Kreisel, A.M. Glazer, G. Jones, P.A. Thomas, L. Abello, G. Lucazeau, J. Phys. Cond. Matt., 12 (2000) 3267-3280.
[52] J. Kreisel, A.M. Glazer, P. Bouvier, G. Lucazeau, Phys. Rev. B, 63 (2001).
[53] M.L. Sanjuan, V.M. Orera, R.I. Merino, J. Blasco, J. Phys. Cond. Matt., 10 (1998) 11687-11702.
[54] T. Inagaki, K. Miura, H. Yoshida, J. Fujita, M. Nishimura, Solid State Ionics, 118 (1999) 265-269.
[55] R. Selvamani, G. Singh, V. Sathe, V.S. Tiwari, P.K. Gupta, J. Phys. Cond. Matt., 23 (2011).
[56] Y.I. Yuzyuk, E. Gagarina, P. Simon, L.A. Reznitchenko, L. Hennet, D. Thiaudiere, Phys. Rev. B, 69 (2004) 7.
[57] Y.D. Juang, S.B. Dai, Y.C. Wang, W.Y. Chou, J.S. Hwang, M.L. Hu, W.S. Tse, Solid State Commun., 111 (1999) 723-728.
[58] T. Noma, S. Wada, M. Yano, T. Suzuki, J. Appl. Phys., 80 (1996) 5223-5233.
[59] Y. Shiratori, C. Pithan, J. Dornseiffer, R. Waser, J. Raman. Spec., 38 (2007) 1288-1299.
[60] P.W. Dunne, A.M. Carnerup, A. Wegrzyn, S. Witkowski, R.I. Walton, J. Phys. Chem. C, 116 (2012) 13435-13445.
[61] Y. Takahashi, H. Sakami, M. Nomura, Anal. Chim. Acta, 468 (2002) 345-354.
[62] S. Skanthakumar, L. Soderholm, Phys. Rev. B, 53 (1996) 920-926.
[63] A. Feteira, D.C. Sinclair, M.T. Lanagan, J. Appl. Phys., 101 (2007) 7.
[64] S.E. Ashbrook, L. Le Polles, R. Gautier, C.J. Pickard, R.I. Walton, Phys. Chem. Chem. Phys., 8 (2006) 3423-3431.
[65] I.P. Aleksandrova, A.A. Sukhovsky, Y.N. Ivanov, Y.E. Yablonskaya, S.B. Vakhrushev, Ferroelectrics, 378 (2009) 16-22.

[66] M. Kotecha, S. Chaudhuri, C.P. Grey, L. Frydman, J. Am. Chem. Soc., 127 (2005) 16701-16712.
[67] G.K.L. Goh, F.F. Lange, S.M. Haile, C.G. Levi, J. Mater. Res., 18 (2003) 338-345.
[68] A.T. Chien, X. Xu, J.H. Kim, J. Sachleben, J.S. Speck, F.F. Lange, J. Mater. Res., 14 (1999) 3330-3339.
[69] H. Jiang, N. Kumada, Y. Yonesaki, T. Takei, N. Kinomura, M. Yashima, M. Azuma, K. Oka, Y. Shimakawa, Jap. J. Appl. Phys., 48 (2009).
[70] U.Y. Hwang, H.S. Park, K.K. Koo, J. Am. Ceram. Soc., 87 (2004) 2168-2174.
[71] A.Z. Simoes, F. Moura, T.B. Onofre, M.A. Ramirez, J.A. Varela, E. Longo, J. Alloys Compd., 508 (2010) 620-624.

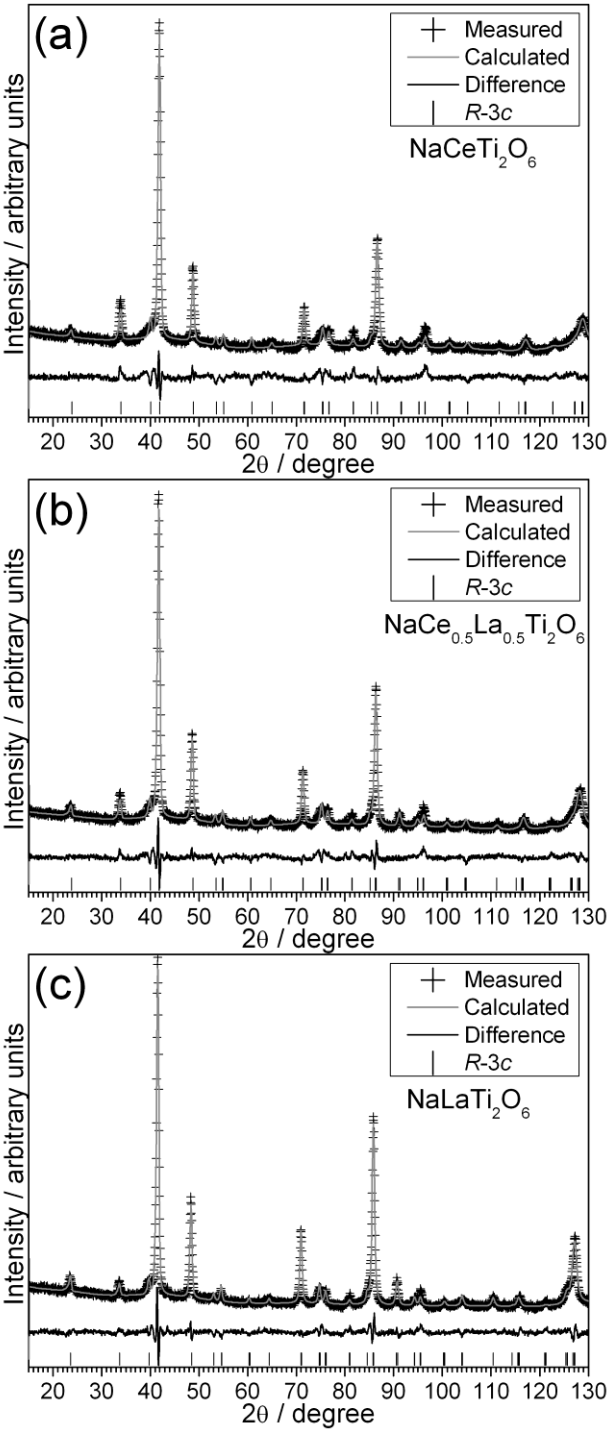

Fig. 1 Rietveld refinement of neutron diffraction of (a) $NaCeTi_2O_6$ (b) $NaCe_{0.5}La_{0.5}Ti_2O_6$ and (c) $NaLaTi_2O_6$, with the points showing the measured neutron diffraction pattern, grey line for calculated, black for the difference and the tick marks shows the peak positions for $R\bar{3}c$ space group.

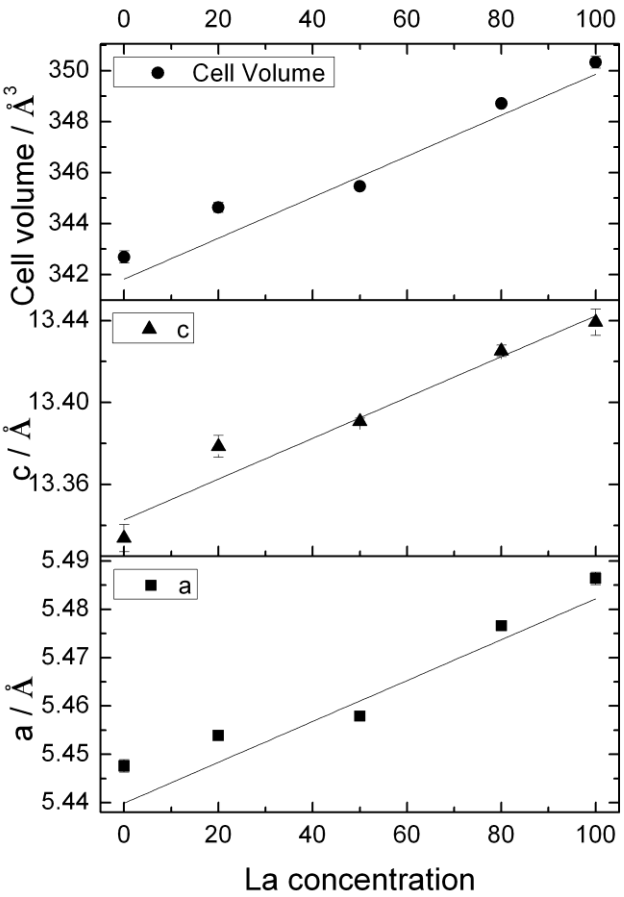

Fig. 2 Plot of the lattice parameters and cell volume of $NaCe_{1-x}La_xTi_2O_6$ series calculated by combined analysis of the neutron and XRD powder data.

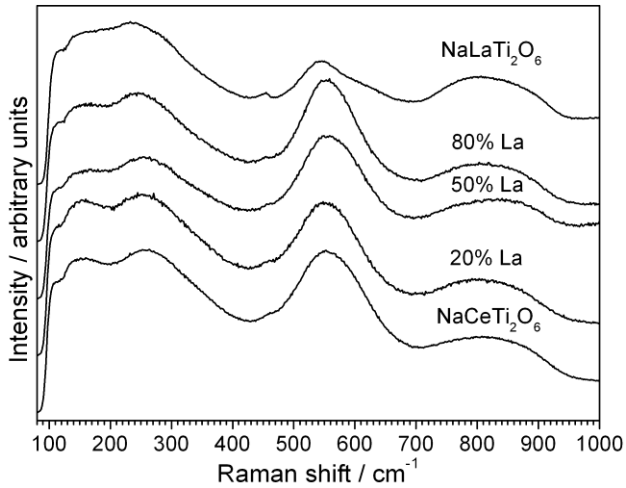

Fig. 3 Raman spectra of $NaCe_{1-x}La_xTi_2O_6$.

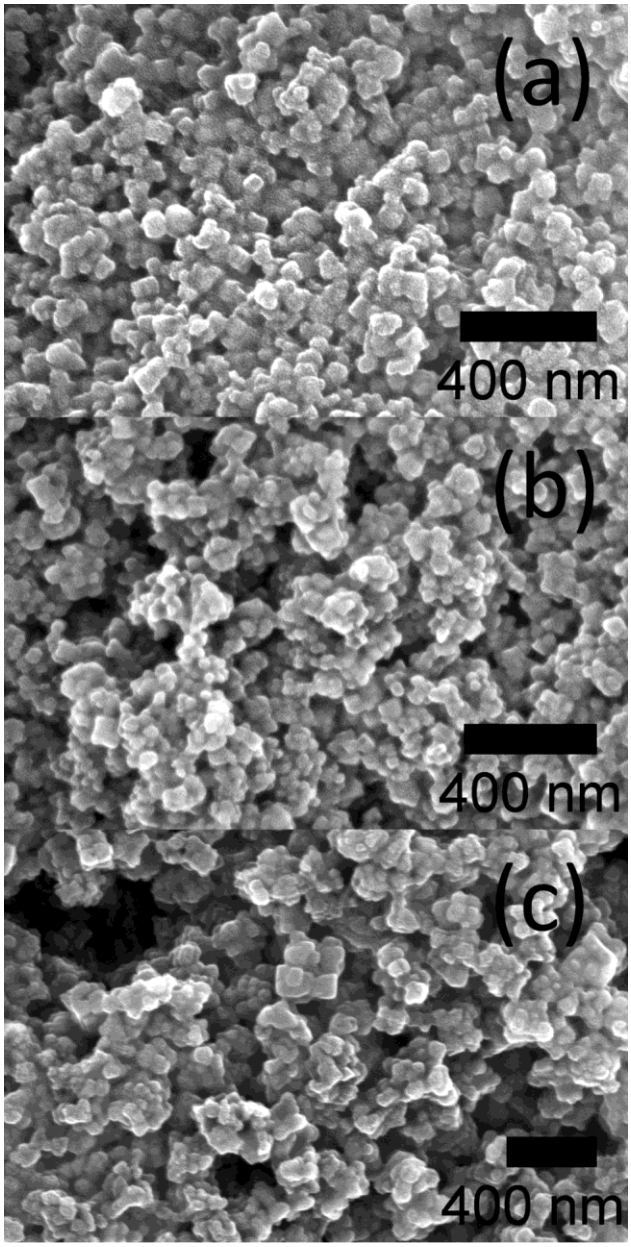

Fig. 4 SEM images of (a) $NaCeTi_2O_6$, (b) $NaCe_{0.5}La_{0.5}Ti_2O_6$ and (c) $NaLaTi_2O_6$ synthesised in 4 M NaOH solution under hydrothermal conditions.

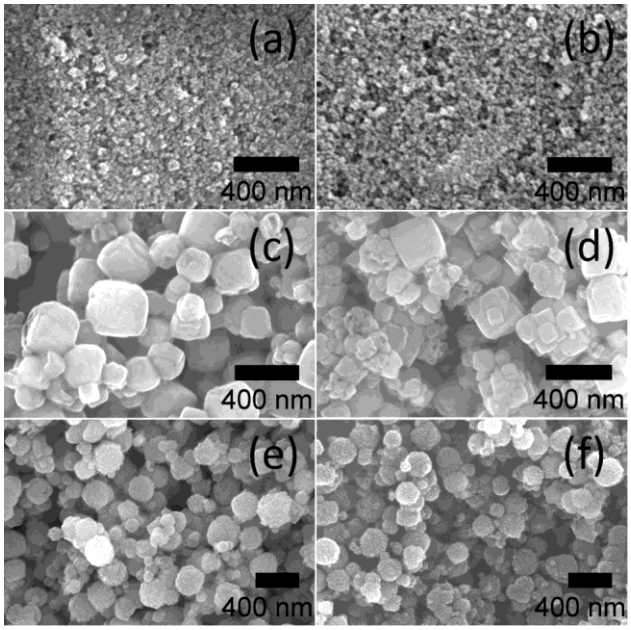

Fig. 5 SEM images of $NaCeTi_2O_6$ and $NaLaTi_2O_6$ powders prepared in (a) and (b) ethylene glycol, (c) and (d) 12 M NaOH and (e) and (f) ethylene glycol and water mixture, respectively.

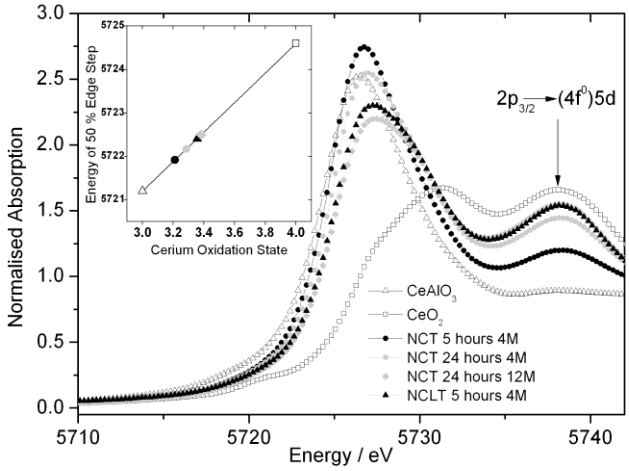

Fig. 6 Ce L_{III}-edge XANES spectra of $NaCeTi_2O_6$ and Ce reference materials with known oxidation state. NCT = $NaCeTi_2O_6$ and NCLT = $NaCe_{0.5}La_{0.5}Ti_2O_6$. The inset shows the correlation between oxidation state and edge position, with deduced average oxidation states of the NCT and NCLT materials labelled using the same symbols as in the main figure.

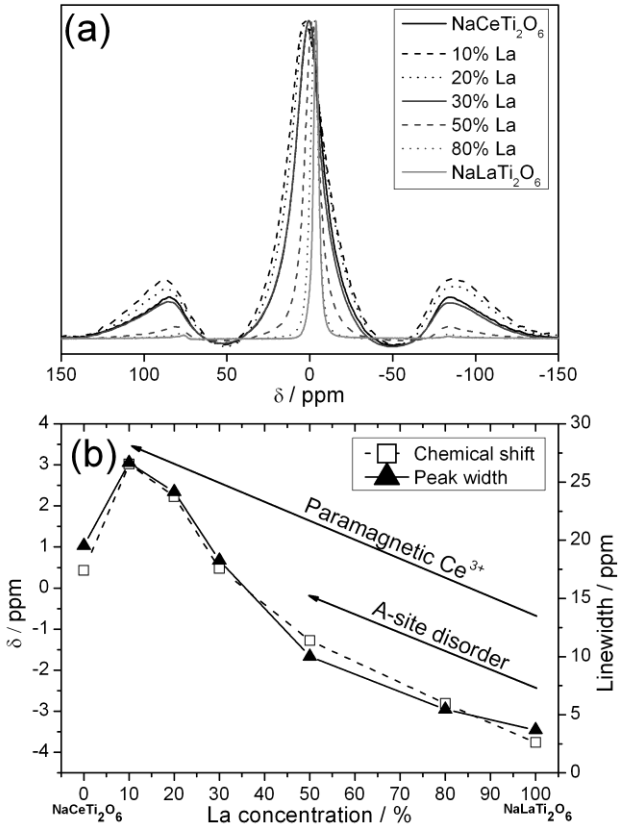

Fig. 7 (a) ^{23}Na NMR (14.1 T) of $NaCe_{1-x}La_xTi_2O_6$ series, (b) plot of the chemical shift and linewidth extracted from the spectra.

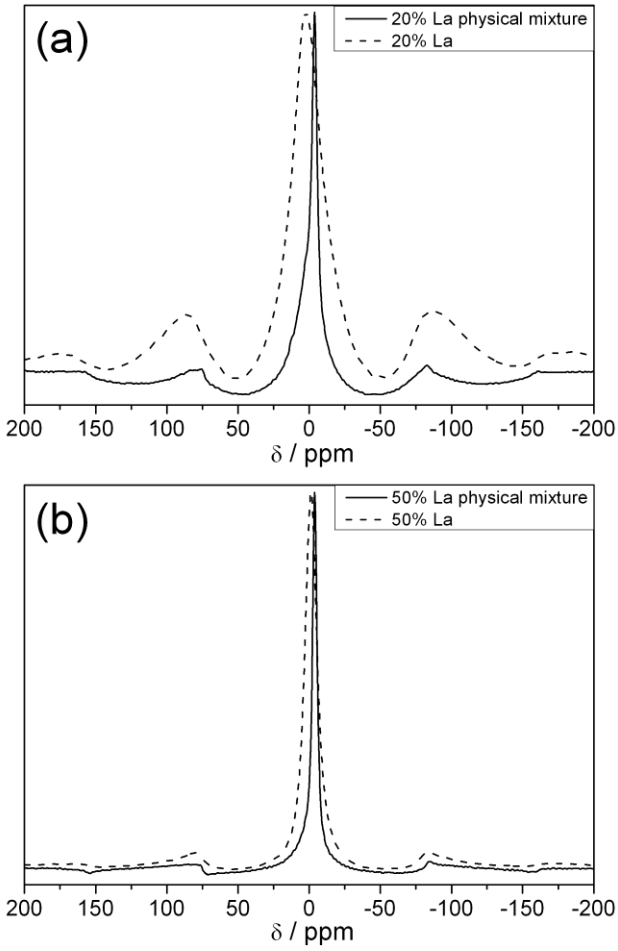

Fig. 8 ^{23}Na (14.1 T) MAS NMR of $NaCe_{1-x}La_xTi_2O_6$ with (a) 20% and (b) 50% La, comparing spectra from perovskite solid solutions and physical mixtures of the pure end members with the same compositions.

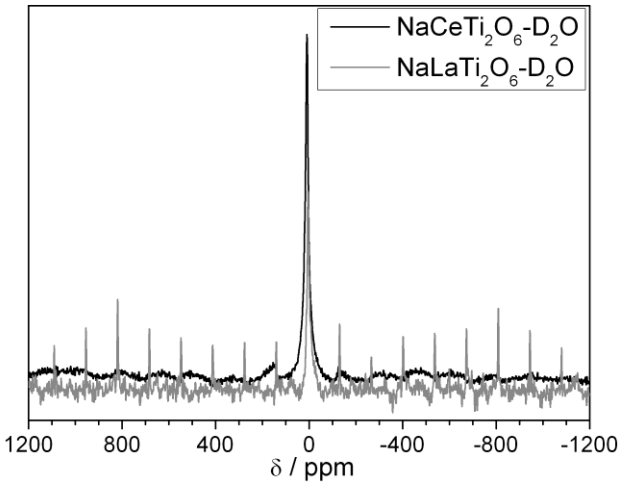

Fig. 9 ^{2}H (14.1 T) MAS NMR of deuterated $NaCeTi_2O_6$ and $NaLaTi_2O_6$ prepared in D_2O and NaOD. Spectra were recorded under conditions that enabled quantitative analysis, by comparison to (natural-abundance) ^{2}H NMR spectra of H_2O.

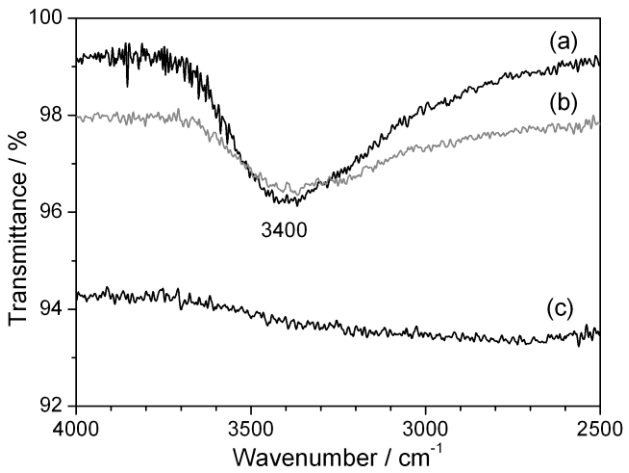

Fig. 10 IR spectra of (a) $NaLaTi_2O_6$, (b) $NaCeTi_2O_6$, and (c) $NaLaTi_2O_6$ after heating at 1100 ^{o}C.